NANO LETTERS

2008
Vol. 8, No. 12
4265-4269

In-Fiber Semiconductor Filament Arrays

D. S. Deng,[†,‡] N. D. Orf,[†,‡] A. F. Abouraddy,[†] A. M. Stolyarov,[§] J. D. Joannopoulos,[†,||] H. A. Stone,[§] and Y. Fink*[,†,‡]

Research Laboratory of Electronics, Department of Materials Science and Engineering, Department of Physics, Massachusetts Institute of Technology, 77 Massachusetts Avenue, Cambridge, Massachusetts 02139, and School of Engineering and Applied Sciences, Harvard University, Cambridge, Massachusetts 02138

Received July 6, 2008; Revised Manuscript Received September 6, 2008

ABSTRACT

We report a novel physical phenomenon in which a cylindrical shell undergoing a scaling process evolves into an ordered array of filaments upon reaching a characteristic thickness. We observe that the tendency to breakup is related to the material viscosity in a manner reminiscent of capillary instability. However, unlike the classical breakup of a fluid cylinder into droplets, the structural evolution in our system occurs exclusively in the cross sectional plane while uniformity is maintained in the axial direction. We propose a fluid front instability mechanism to account for the observed phenomena. The fleeting evolution of fluid breakup from a thin film to a filament array is captured in the frozen state by a thermal drawing process which results in extended lengths of solid sub-100 nm filaments encapsulated within a polymer fiber. Hundreds of glassy semiconductor filament arrays are precisely oriented within a polymer fiber matrix making electrical connections trivial. This approach offers unique opportunities for fabrication of nanometer scale devices of unprecedented lengths allowing simplified access and connectivity.

Optical-fiber thermal drawing from a viscous macroscopic preform is a well-established process for producing kilometer-long silica fibers with uniform dimensions in the telecommunication industry.[1,2] In the past decade, microstructured fibers incorporating air enclaves have been created with these methods, resulting in novel fiber designs.[3−8] All these fibers, however, consist of a single material with the possible addition of air cavities. The fact that these fibers consist of a single dielectric material limits their usage to optical-transport related applications.

An altogether different class of fibers incorporating multiple materials (e.g., semiconductors, insulators, and metals) thermally drawn from a macroscopic preform has recently emerged.[9−16] These fibers allow one, in principle, to incorporate the functionality of a semiconductor device into a fiber. The straightforward fabrication process has four main steps (see Figure 1a). (i) An amorphous semiconductor film of desired thickness is thermally evaporated onto an amorphous polymer substrate. (ii) The semiconductor/polymer bilayer film is tightly wrapped around a polymer tube. (iii) Additional layers of protective polymer cladding are then rolled around the structure. (iv) The preform is fused into a single solid structure by heating under vacuum. The solid preform is then heated into the viscous state and controllably stretched into an extended fiber by application of axial tension.

Fibers with layered structures have been successfully achieved with this unique method.[4−6] Tens-of-meters long fibers with a uniform diameter have been produced, as seen from the inset of Figure 1a (iv). The cross-section and semiconductor layer of fiber (see Figure 1c) do not change during drawing; they are simply a scaled-down version of preform structure (Figure 1b). The semiconductor film geometry is important in structures such as cylindrical multilayer photonic bandgap fibers[9,10] and sensitive optical and thermal fiber detectors.[11−13]

Increasing the number of semiconductor devices incorporated into a single fiber is desirable for enabling multiple functionalities. This objective naturally entails a decrease in feature dimensions. However, what happens to extremely thin films during the top-down thermal drawing process has not been explored. One may reasonably expect that surface-energy-driven instabilities while the preform is in the viscous fluid state will impact the resulting geometry. In fact, this approach may be viewed as a test bed for studying such instabilities with several distinct and unique advantages. The effect of shrinking the liquid film (or other structures of interest) may be studied over a very wide range of parameters and can be finely controlled during the fiber-drawing process. The produced structures are "frozen" into the fiber so that they may be directly observed by both cross-sectional and axial inspection, and quantitative conclusions concerning stability limits of the feature size can be made.

* To whom correspondence should be addressed. E-mail: yoel@mit.edu.
† Research Laboratory of Electronics, Massachusetts Institute of Technology.
‡ Department of Materials Science and Engineering, Massachusetts Institute of Technology.
§ Harvard University.
|| Department of Physics, Massachusetts Institute of Technology.

10.1021/nl801979w CCC: $40.75
Published on Web 10/29/2008

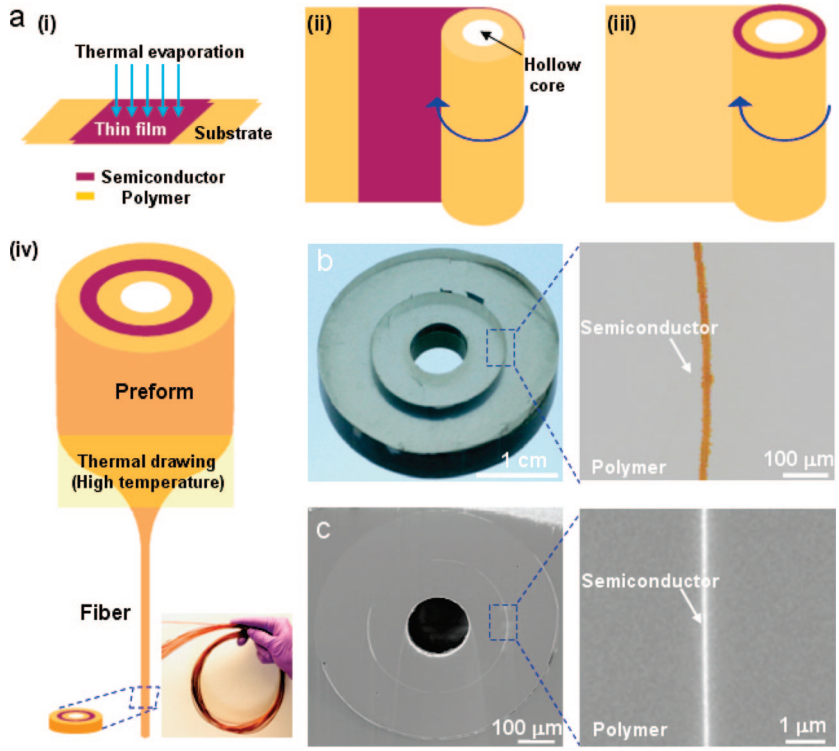

Figure 1. Preform-to-fiber fabrication process. (a) (i) Thermal evaporation of a glass film on a polymer substrate; (ii) wrapping film around polymer rod with a hollow core; (iii) cladding the film with polymer matrix; (iv) thermal drawing from preform to fiber with the layer structure retained. Inset is photograph of tens-of-meters long fiber. (b) An optical microscope image of the layer structure in the preform is shown on the left, and a magnified section of the thin film on the right. (c) SEM micrograph of the fiber cross-section is shown on the left, and a magnified section of the intact semiconductor thin film, right, confirms that the layered structure is preserved.

To investigate the smallest achievable thickness of the thin film, we have studied multiple material combinations. Two amorphous semiconductors (Se and As_2Se_3) and two polymers (polysulfone, PSU, and polyethersulfone, PES) were used in two combinations (Se with PSU and As_2Se_3 with PES). The materials in the pairings have similar thermomechanical properties in an overlapping temperature range as well as good adhesion through repeated thermal cycling, both properties being crucial to facilitate codrawing of the two different materials.[14,15]

To isolate the effect of film thickness, a fiber preform consisting of several concentric amorphous semiconductor films having decreasing thicknesses was prepared for each material combination (as depicted schematically in Figure 2a). The preform was consolidated under vacuum for approximately one hour at ~260 or 220 °C for As_2Se_3/PES and Se/PSU combinations, respectively. To draw tens of meters of fiber from cylindrical preforms measuring 160 mm in length and 20 mm in diameter, a conventional optical fiber draw tower consisting of a three-zone furnace to heat the preform to its processing temperature (high-temperature zone set to ~300 °C for As_2Se_3/PES and ~260 °C for Se/PSU fibers), a feeding process to controllably introduce the preform into the furnace (downfeed speed of 0.003 mm·s^{-1}), and a capstan to pull the resulting fiber from the preform (set at was ~0.1 m·min^{-1}) were used. The drawing parameters were fixed to keep a constant draw-down ratio of about 20 between the feature sizes of the initial preform and final fiber.

SEM micrographs of a fiber cross-section (Figure 2b) show that the thicker semiconductor layers remain intact after drawing, but thinner layers break up. A striking difference in film stability is highlighted in the magnified fiber cross-sections for Se/PSU (Figure 2c) and As_2Se_3/PES (Figure 2d). Only the thickest Se layer remains intact after drawing while the three thinner layers undergo different degrees of circumferential breakup (Figure 2c). The thinnest Se layer completely breaks up into circular features. In contrast, all the As_2Se_3 layers remain intact above 10 nm with layer breakup occurring only in the thinnest 3-nm layer (Figure 2d). Additionally, the average spacing between Se segments in Figure 2c is found to be linearly proportional to the layer thickness (inset of Figure 2b).

Given these observations of circumferential layer breakup in the fiber, the question of axial stability naturally arises. To facilitate the observation of the axial behavior, we prepared two new preforms, each with a single thin Se films (Figure 3a). One preform contains a thin Se film with a final dimension after fiber drawing of sub-100 nm and is expected to break up (Figure 3b,c). The second preform has a final thickness after drawing of 800 nm and is expected to remain intact (Figure 3d,e). Photographs in Figure 3b,d demonstrate the color and mechanical flexibility of the fibers. Axial inspection of the fibers reveals continuous Se filaments form in the sub-100-nm layer fiber (Figure 3c); the 800-nm larger fiber remains intact as amorphous state,[17,18] (Figure 3e). The

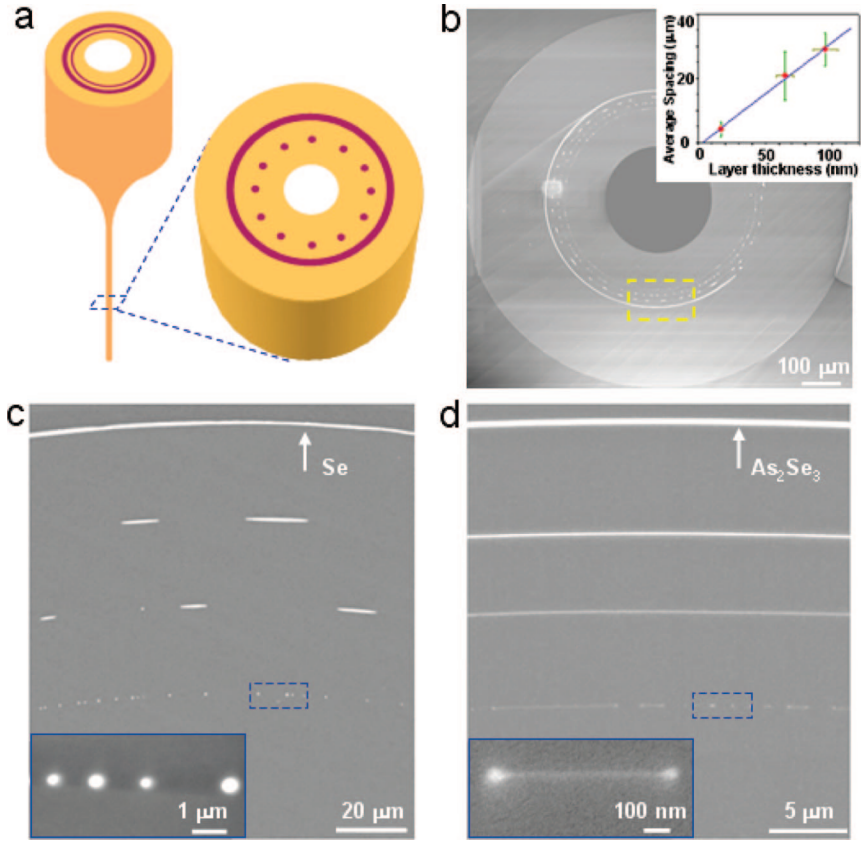

Figure 2. Breakup of layers at the nanometer scale. (a) Sketch of the preform with multiple films of decreasing thickness and fiber cross-section indicating breakup of thinner layers. (b) An SEM micrograph of a fiber cross-section; inset showing that average spacing of break-up segments varies linearly with the final layer thickness. (c) Magnification of Se/PSU fiber cross-section (boxed area in panel b) (the final layer thicknesses in fiber are 700, 96, 65, and 17 nm, respectively) showing that the layers are broken when pulled to below 100 nm thickness; inset for a further magnified section of the 17 nm layer. (d) Magnification of As_2Se_3/PES fiber cross-section (the final layer thicknesses in fiber are 270, 70, 14, and 3 nm, respectively) showing that the layers are maintained to sub-15 nm thickness; inset shows a further magnified section of the 3 nm layer.

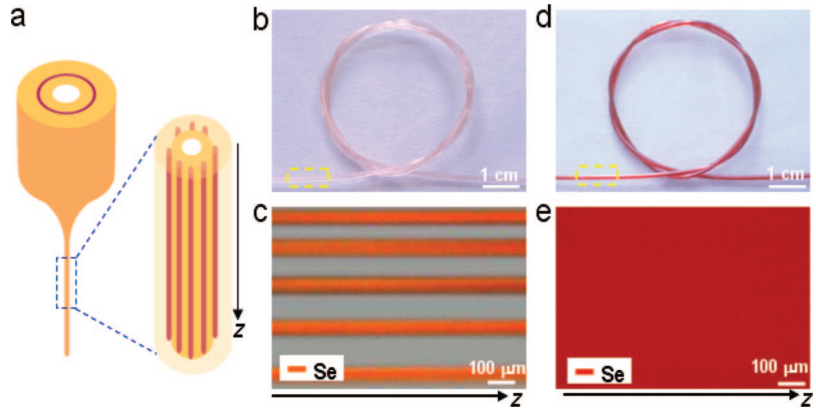

Figure 3. Extended and ordered filament arrays embedded in the fiber. (a) Sketch of the preform with a thin film and fiber with the extended filaments after layer breakup. (b) Photograph of a Se/PSU fiber exhibiting cross-sectional break-up of the sub-100-nm layer. (c) Optical microscope image (boxed area in panel b) taken along the length of fiber revealing extended amorphous Se filaments embedded in this fiber. (d,e) Photograph and optical microscope image of a Se/PSU fiber with a thick Se film that does not breakup.

reproducibility of the extended filaments has been confirmed by several independent fiber drawings in both Se/PSU and As_2Se_3/PES system. We have not found any axial filament breakup, though branching and recombination of the filaments appear occasionally due to defects or in homogeneities in the prepared thin film. Thus, the well-ordered parallel filament arrays span the entire fiber length. Combining the cross-sectional (Figure 2c) and axial (Figure 3c) observation of the filament, we conclude that the *a*-Se and As_2Se_3 filaments have ribbon-like three-dimensional structures (approximately 100 nm × 10 μm × length and 20 nm × 20 nm × length of fiber, respectively).

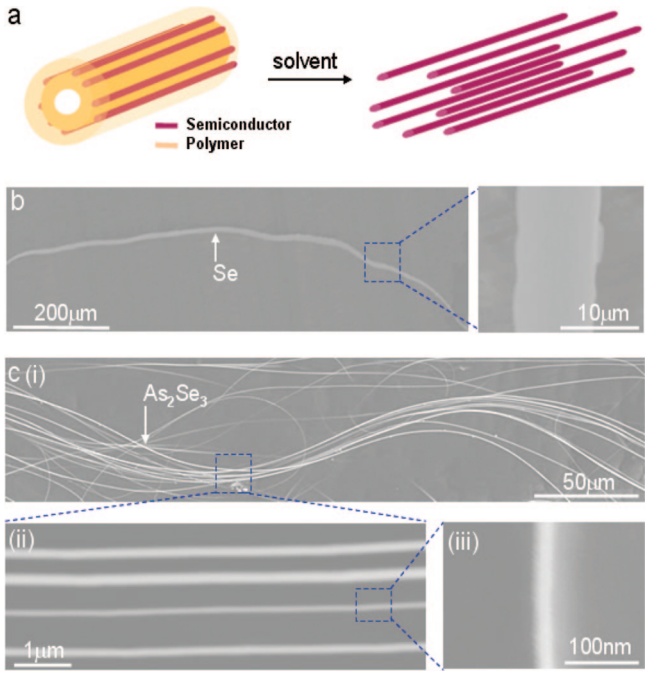

Figure 4. Semiconductor nanofilaments extracted from fiber. (a) The filament bundles are extracted from the fiber by dissolving the polymer matrix. (b) SEM micrograph of a Se filament and a magnified section of it. (c) (i) A bundle of As_2Se_3 filaments. (ii) Magnified section showing parallel filaments. (iii) A section of a single filament.

An intriguing feature of this phenomenon is the potential use of these semiconductor filaments after extraction from the polymer matrix (Figure 4a). Indeed, the polymer matrix is easily dissolved away by a solvent (dimethylacetamide), leaving filament arrays for possible further processing. Examples of the extracted filaments are given in Figure 4b,c. Figure 4b shows a 1-mm long Se filament extracted from a fiber composed of 100 nm thick Se layer that has broken up (the same fiber as Figure 3c). A bundle of As_2Se_3 filaments extracted from an As_2Se_3/PES fiber (from a single As_2Se_3 thin-film preform) is shown in Figure 4c. Individual filaments have sub-100-nm width and 10-nm thickness.

The length of nanofilaments produced with this method is especially captivating.[19−21] For example, the semiconductor film in a typical fiber preform is 10-cm long, 3-cm wide (the preform circumference) and hundreds of nanometers in thickness (these dimensions are by no means limits, but are simply experimentally convenient). From this preform, forty meters of fiber may be produced if it is drawn down by a scaling factor of 20. The number of filaments in the fiber is around 100 (diameter of fiber is 1 mm and spacing between filaments is around 10 μm). Thus hundreds of meters long filaments can possibly be produced from a single semiconductor sheet clad in a polymer preform. This unique feature is due to the transition in dimensionality from a 2D sheet into 1D filament arrays. Furthermore, because the fiber dimensions may be easily changed and the fiber drawing process may have draw-down ratios much greater than 20, hundreds-of-meters long nanofilaments may possibly be many orders of magnitude longer than other approaches to nanowire production. Note that this is achieved in the form of hundreds of nanofilaments all possessing the same global orientation inside the fiber.

The breakup mechanism of the sheet into filament arrays is not completely understood at this point (see Figure 5a).[22−24] We proceed to outline a fluid-front instability mechanism as a heuristic model to explain these observations. This mechanism is based on the classical capillary instability model.[25,26] First, we note that the thin semiconductor glass film does not extend along the entire length of the preform. At the beginning of thermal drawing, only polymer is located in the high-temperature zone where the preform deforms in the viscous state. At this time, the film is outside the high-temperature zone. As the drawing proceeds, the part of the preform containing the film is gradually fed into the high-temperature zone and a viscous glass/polymer interface is formed. We assume this interface has a curved fluid front due to interfacial tension (with a radius of curvature r that is approximately half of the glass layer thickness h, $r \sim h/2$, as seen in Figure 5b(i)).[23,27] A capillary instability develops on this curved front where small initial perturbations grow rapidly into protrusions (Figure 5b(ii)). These protrusions extend into filaments along the axial direction as the rest of the preform passes into the high-temperature region. The

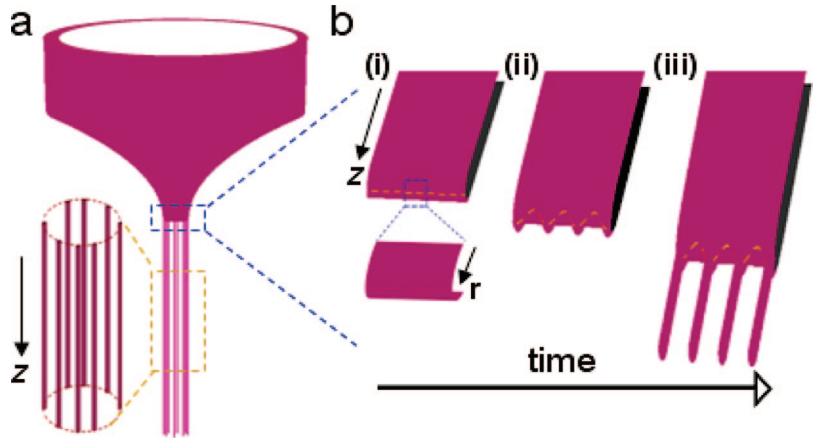

Figure 5. Proposed mechanism of filament arrays formation. (a) Schematic of a layer breakup into filaments during drawing. (b) (i−iii) A schematic of the time evolution of layer breakup. The formed viscous polymer/viscous glass interface has a cylindrical fluid front, whose breakup is driven by capillary instability.

filaments subsequently freeze in place as the fiber emerges from the high-temperature zone and cools (Figure 5b(iii)).

The predictions based on this mechanism qualitatively agree with our experimental results. The linear theory of capillary instability, such as the classic Rayleigh and Tomotika models, states that the capillary instability growth rate σ is proportional to the interfacial tension γ, and inversely proportional to the viscosity η and layer thickness h.[25,26] For any given material system, thinner layers have shorter instability time corresponding to a large growth rate and are therefore unstable during fiber drawing as observed in Figure 2. Furthermore, this capillary instability predicts the linear relationship between the average spacing and the layer thickness, which is consistent with the experimental observations (inset of Figure 2b). For the two different materials systems we have considered, Se/PSU and As_2Se_3/PES, Se has 5 orders-of-magnitude lower viscosity than that of As_2Se_3,[28] so Se layers are more vulnerable to breakup than As_2Se_3 layers, as seen in Figure 2. One may expect that surface tension should result in the cylindrical filaments (Figure 2c inset) breaking up axially into droplets. However, axial tension and viscous boundaries may contribute to stabilizing the filament leading to a time scale for axial breakup, which is longer than that of circumferential breakup. This is confirmed by the fact that we have not observed axial breakup in our experiments.

Several other candidate mechanisms are less likely to contribute to the observed behavior but warrant further exploration. First, the dewetting instability[29] of thin films (resulting from the van der Waals forces) acts at a short-range ($\sim$10 nm) and hence does not play an important role in our experiments where the glass fluid front thickness is on the order of micrometers in the high-temperature zone. A second candidate is the Saffman−Taylor instability in which a low-viscosity fluid (the glass thin film in our case) is pushed into a high-viscosity fluid (the polymer cladding).[30] Future studies will further elucidate the detailed instability mechanism by using a wider class of materials and by building a comprehensive model that includes additional effects such as thermal diffusion and axial stretching.

This top-down methodology (macroscopic preform to microscopic fiber to nanoscale filaments) is a unique approach to producing nanofilaments with several attractive features. These filaments may be produced in a high-throughput and low-cost fashion. The arrays are well-ordered with parallel alignment. Furthermore, these filaments are encapsulated in a protective polymer matrix, which lends itself to manual manipulation until the need to extract the filaments arises. We thus bypass the fragility of these nanostructures during handling that plagues other approaches. Most importantly, the nanofilaments are produced with exceptionally long lengths. Nanofilaments may be potentially useful in enabling large-area applications including renewable energy (photovoltaics, thermoelectrics) and bioengineering (scaffolding for tissue growth). Directions for future work include producing high-density filament bundles using a multiplicity of layers in the fiber preform, and assembling metal and semiconductor structures in the same fiber.

Acknowledgment. We thank Shandon Hart, Zheng Wang, Fabien Sorin, and Gareth McKinley for helpful discussions at different stages of this work. We acknowledge Steve Kooi for help with the SEM micrographs. This work was supported by the Center for Materials Science and Engineering at MIT, as part of the MRSEC Program of the National Science Foundation under award number DMR 02-13282. This research was supported (in part) by the U.S. Army through the Institute for Soldier Nanotechnologies, under Contract W911NF-07-D-0004 with the U.S. Army Research Office.

References

(1) Keck, D. B.; Maurer, R. D.; Schultz, P. C. *Appl. Phys. Lett.* **1973**, *22*, 307–309.
(2) Agrawal, G. P. *Fiber-optic communication systems*, 3rd ed.; Wiley-Interscience: New York, 2002.
(3) Broeng, J.; Mogilevstev, D.; Barkou, S. E.; Bjarklev, A. *Opt. Fiber Technol.* **1999**, *5*, 305–330.
(4) Eggleton, B. J.; Kerbage, C.; Westbrook, P. S.; Windeler, R. S.; Hale, A. *Opt. Express* **2001**, *9*, 698–713.
(5) van Eijkelenborg, M. A.; Large, M. C. J.; Argyros, A.; Zagari, J.; Manos, S.; Issa, N. A.; Bassett, I.; Fleming, S.; McPhedran, R. C.; de Sterke, C. M.; Nicorovici, N. A. P. *Opt. Express* **2001**, *9*, 319–327.
(6) Allan, D. C. et al. In *Photonic Crystals and Light Localization in the 21st Century ed.*; Soukoulis, C. M., Ed.; Kluwer Academic: Dordrecht, 2001; pp 305−320.
(7) Knight, J. C. Photonic crystal fibres. *Nature* **2003**, *424*, 847–851.
(8) Joannopoulos, J. D.; Johnson, S. G.; Meade, R. D.; Winn, J. N. *Photonic crystals: Molding the flow of light*; 2nd ed.; Princeton University Press; NJ, 2008.
(9) Hart, S. D.; Maskaly, G. R.; Temelkuran, B.; Prideaux, P. H.; Joannopoulos, J. D.; Fink, Y. *Science* **2002**, *296*, 510–513.
(10) Temelkuran, B.; Hart, S. D.; Benoit, G.; Joannopoulos, J. D.; Fink, Y. *Nature* **2002**, *420*, 650–653.
(11) Bayindir, M.; Sorin, F.; Abouraddy, A. F.; Viens, J.; Hart, S. D.; Joannopoulos, J. D.; Fink, Y. *Nature* **2004**, *431*, 826–829.
(12) Bayindir, M.; Shapira, O.; Saygin-Hinczewski, D.; Viens, J.; Abouraddy, A. F.; Joannopoulos, J. D.; Fink, Y. *Nat. Mater.* **2005**, *4*, 820–825.
(13) Abouraddy, A. F.; Shapira, O.; Bayindir, M.; Arnold, J.; Sorin, F.; Hinczewski, D. S.; Joannopoulos, J. D.; Fink, Y. *Nat. Mater.* **2006**, *5*, 532–536.
(14) Bayindir, M.; Abouraddy, A. F.; Shapira, O.; Viens, J.; Saygin-Hinczewski, D.; Sorin, F.; Arnold, J.; Joannopoulos, J. D.; Fink, Y. *IEEE J. Sel. Top. Quantum Electron.* **2006**, *12*, 1202–1213.
(15) Abouraddy, A. F.; Bayindir, M.; Benoit, G.; Hart, S. D.; Kuriki, K.; Orf, N.; Shapira, O.; Sorin, F.; Temelkuran, B.; Fink, Y. *Nat. Mater.* **2007**, *6*, 336–347.
(16) Sorin, T.; Abouraddy, A. F.; Orf, N.; Shapira, O.; Viens, J.; Arnold, J.; Joannopoulos, J. D.; Fink, Y. *Adv. Mater.* **2007**, *19*, 3872–3877.
(17) Li, Q.; Yam, V. W. W. *Chem. Commun.* **2006**, *9*, 1006–1008.
(18) Lee, J. H.; Kim, M. G.; Yoo, B. Y.; Myung, N. V.; Maeng, J. S.; Lee, T.; Dohnalkova, A. C.; Fredrickson, J. K.; Sadowsky, M. J.; Hur, H. G. *Proc. Natl. Acad. Sci. U.S.A.* **2007**, *104*, 20410–20415.
(19) Hu, J. T.; Odom, T. W.; Lieber, C. M. *Acc. Chem. Res.* **1999**, *32*, 435–445.
(20) Xia, Y. N.; Yang, P. D.; Sun, Y. G.; Wu, Y. Y.; Mayers, B.; Gates, B.; Yin, Y. D.; Kim, F.; Yan, Y. Q. *Adv. Mater.* **2003**, *15*, 353–389.
(21) Wang, Z. L. *Annu. Rev. Phys. Chem.* **2004**, *55*, 159–196.
(22) Eggers, J. *Rev. Mod. Phys.* **1997**, *69*, 865–929.
(23) de Gennes, P. G.; Brochard-Wyart, F.; Quere, D. *Capillarity and Wetting phenomena*; Springer: New York, 2002.
(24) Lin, S. P. *Breakup of Liquid Sheets and Jets*; Cambridge University Press; Cambridge, England, 2003.
(25) Rayleigh, L. *Proc. London. Math. Soc.* **1878**, *10*, 4–13.
(26) Tomotika, S. *Proc. R. Soc. London A* **1935**, *150*, 322–337.
(27) Leizerson, I.; Lipson, S. G.; Lyushnin, A. V. *Langmuir* **2004**, *20*, 291–294.
(28) Tverjanovich, A. S. *Glass Phys. Chem.* **2003**, *29*, 532–536.
(29) Reiter, G. *Phys. Rev. Lett.* **1992**, *68*, 75–78.
(30) Saffman, P. G.; Taylor, G. I. *Proc. R. Soc. London, Ser. A* **1958**, *245*, 312–329.

NL801979W